Title: Simplifying and expanding the scope of boron imidazolate framework (BIF) synthesis using mechanochemistry

Authors: Cameron B. Lennox,[a,b] Jean-Louis Do,[a,b] Joshua G. Crew,[a,c] Mihails Arhangelskis,[a,d] Hatem M. Titi,[a,b] Ashlee J. Howarth,[b,e,f] Omar K. Farha[f] and Tomislav Friščić[a,b]*

[a] Department of Chemistry, McGill University, 801 Sherbrooke St. W. H3A 0B8 Montreal, Canada. E-mail: tomislav.friscic@mcgill.ca
[b] FRQNT Quebec Centre for Advanced Materials (QCAM/CQMF), Montreal, Canada
[c] School of Chemistry, Cardiff University, Main Building, Park Place, Cardiff CF10 3AT, UK
[d] Faculty of Chemistry, University of Warsaw, 1 Pasteura St. 02-093 Warsaw, Poland.
[e] Department of Biochemistry and Chemistry, Concordia University, 7141 Sherbrooke St. W. H4B 1R6 Montreal, Canada.
[f] International Institute for Nanotechnology, Department of Chemistry, Northwestern University, 2145 Sheridan Road, 60208 Evanston, Il, United States

Main text

Mechanochemistry[1–7] has emerged as a versatile methodology for the synthesis and discovery of advanced materials, including nanoparticle systems[8–10] and metal-organic frameworks (MOFs),[11–15] giving rise to materials that are challenging to obtain using conventional solution-based techniques.[16–18] Mechanochemical techniques such as ball milling, twin screw extrusion[19] and acoustic mixing[20,21] have simplified and advanced the synthesis of a wide range of MOFs, permitting the use of simple starting materials such as metal oxides, hydroxides or carbonates,[22,23] at room temperature and without bulk solvents, yielding products of comparable stability and, after activation, higher surface areas than solution-generated counterparts.[24,25]

The advantages of mechanochemistry in MOF synthesis and discovery have led us to address the possibility of synthesizing boron imidazolate frameworks (BIFs),[26] an intriguing but poorly developed class of microporous materials, analogous to zeolitic imidazolate frameworks (ZIFs),[27–29] comprising equimolar combinations of tetrahedrally coordinated boron(III) and monovalent Li^+ or Cu^+ cations as nodes. Although BIFs offer an attractive opportunity to access microporous MOFs with lower molecular weights, particularly in the case of "ultralight" systems based on Li+ and B(III) centers, this family of materials has remained largely unexplored – potentially due to the need for harsh synthesis conditions, including the use of *n*-butyllithium in a solvothermal environment.[29]

We now show how switching to the mechanochemical environment enables lithium- and copper(I)-based BIFs to be prepared rapidly (*i.e.*, in an hour or less), without elevated temperatures or bulk solvents, and from readily accessible solid reactants, such as hydroxides and oxides. While the mechanochemically-prepared BIFs exhibit significantly higher surface areas than the solvothermally-prepared counterparts, mechanochemistry allows for expanding this class of materials towards previously not reported Ag^+ nodes. The introduction of BIFs isostructural with those based on Li^+ or Cu^+ but comprising of Ag^+ ions, enables a periodic density-functional theory (DFT) evaluation of their stability. This reveals that switching to heavier elements as tetrahedral nodes improves the stability of sodalite topology (SOD) open BIFs with respect to close-packed diamondoid (dia) topology polymorphs.

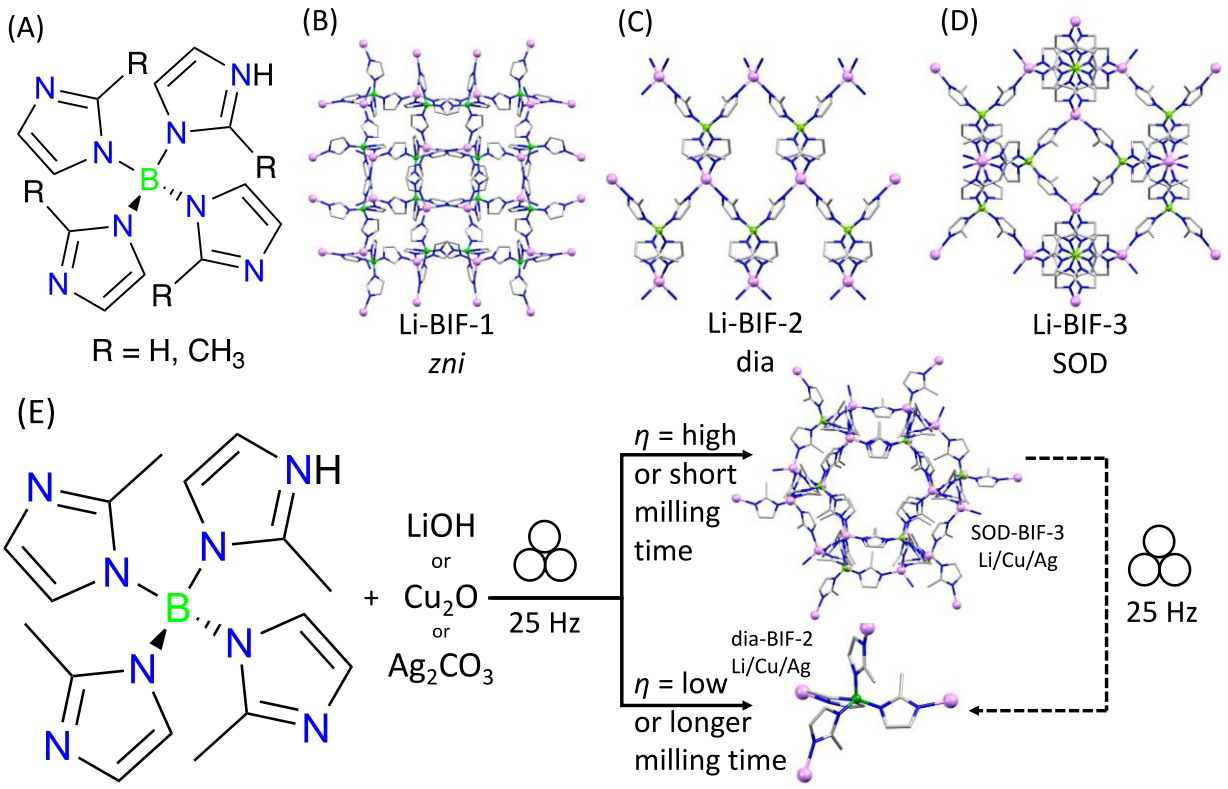

Figure 1. (A) Tetrakis(imidazolo)borate used as reagent to form the closed packed (B) Li-BIF-1 (CSD MOXJEP), (C) Li-BIF-2 (CSD MUCLIG) or porous (C) Li-BIF-3 CSD MUCLOM. (E) Scheme to form precursor extended frameworks with selective porosity based on amount of liquid additive or milling time.

As a first attempt to mechanochemically synthesize BIFs, we explored a formal salt metathesis between either copper(I) chloride or lithium chloride and the commercially available sodium tetrakis(imidazolo)borate (Na[B(**Im**)$_4$]) (Figure 2A). Milling of LiCl and Na[B(**Im**)$_4$] in a 1:1 stoichiometric ratio for up to 60 minutes led to a loss of crystallinity, revealed by the loss of discernible Bragg reflections in powder X-ray diffraction (PXRD) analysis (see ESI). Milling in the presence of a small amount of methanol (MeOH, 120 μL, corresponding to a liquid-to-solid ratio[30] η = 0.5 μL mg-1), however, led to a partial metathesis reaction evident from the appearance of X-ray reflections corresponding to the zni-topology LiB(**Im**)$_4$ (Li-BIF-1), NaCl and residual Na[B(**Im**)$_4$]. Changing the milling liquid to acetonitrile (MeCN) allowed for complete conversion to the desired framework, evidenced by PXRD analysis (Figure 2B-E). Attempts to form the isostructural copper analogue, CuB(**Im**)$_4$ (Cu-BIF-1), under similar liquid-assisted grinding (LAG) conditions using MeOH or MeCN (η = 0.5 μL mg-1) lead to a crystalline product with PXRD reflections matching with CuB(**Im**)$_4$ (Cu-BIF-1), NaCl and residual Na[B(**Im**)$_4$] (see ESI).

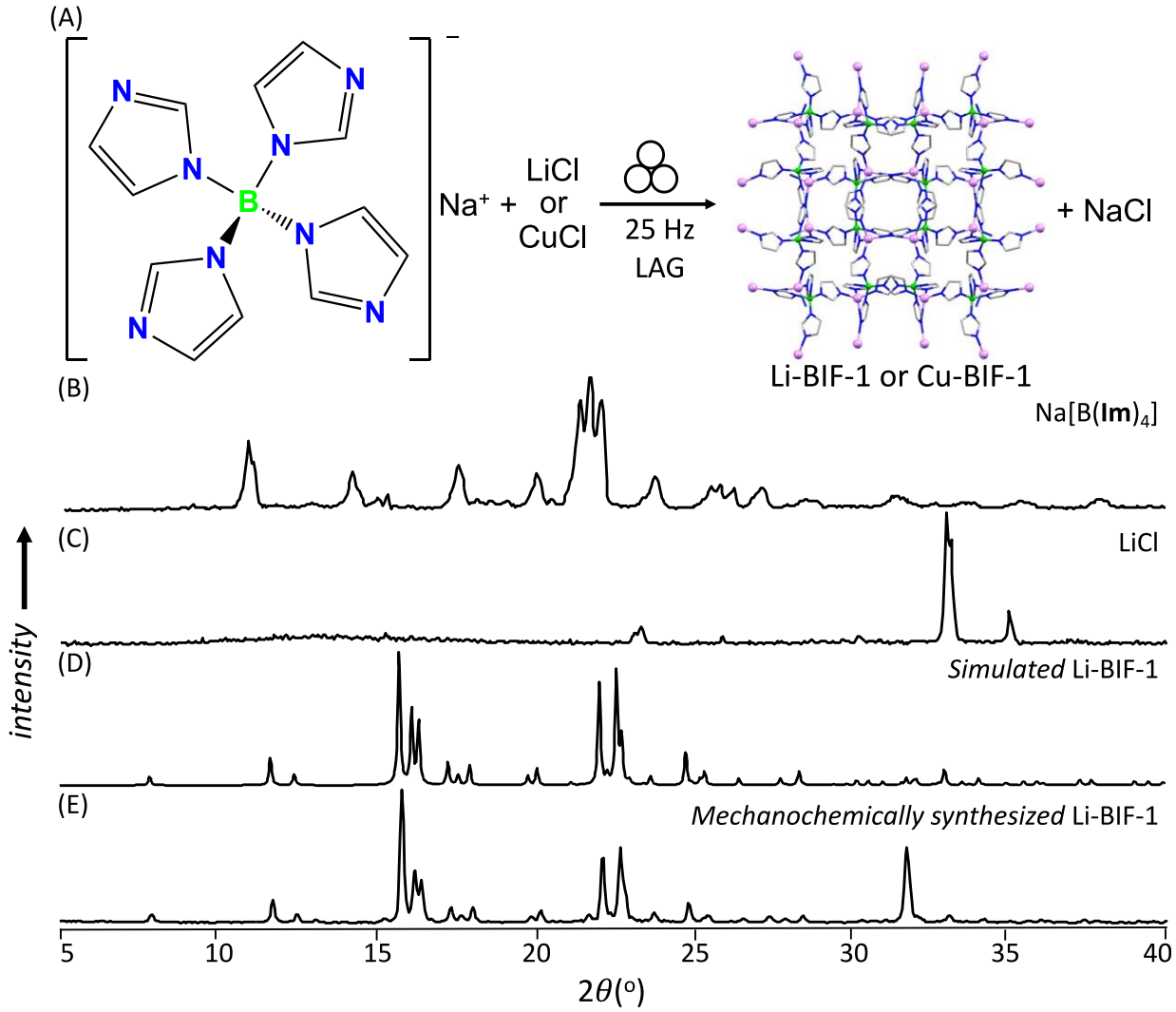

Figure 2. (A) Reaction scheme for the synthesis of Li-BIF-1 by a salt metathesis strategy. Stacked PXRD of (B) Na[B(**Im**)$_4$] (C) LiCl, (D) simulated Li-BIF-1 (CSD MOXJPEP) and (E) synthesized BIF-1-Li by LAG for 60 minutes with MeCN (η=0.5 μL mg-1). Corresponding PXRD patterns for the synthesis of Cu-BIF-1 are given in ESI.

Next, we explored a synthesis approach previously used to form ZIFs and other MOFs: an acid-base reaction[31] of a metal oxide or hydroxide with the pre-synthesized tetrakis(imidazolato)boric acid, HB(**Im**)$_4$ (Figure 3A). Neat milling LiOH with one equivalent of HB(**Im**)$_4$ led to the partial formation of Li-BIF-1, evidenced by PXRD analysis (see ESI). Complete conversion of reactants into Li-BIF-1 was achieved in 60 minutes by LAG in the presence of MeCN (η=0.25 μL mg-1), as evidenced by PXRD analysis (Figure 3B-E), Fourier transform infrared attenuated total reflectance spectroscopy (FTIR-ATR), as well as thermogravimetric analysis (TGA) in air and elemental analysis.

Neat milling of HB(**Im**)$_4$ with Cu_2O under similar conditions yielded a largely non-crystalline material, as evidenced by PXRD (see ESI). However, switching to the ion- and liquid-assisted grinding (ILAG) methodology, in which the reactivity of a metal oxide is enhanced by a weakly acidic ammonium salt,[32-34] enabled the synthesis of BIF-1-Cu from Cu_2O. Specifically, PXRD analysis revealed complete disappearance of the oxide in samples obtained by ILAG with MeOH or MeCN (η = 0.5 μL mg-1) in the presence of 5 mol% NH_4NO_3 (see ESI).

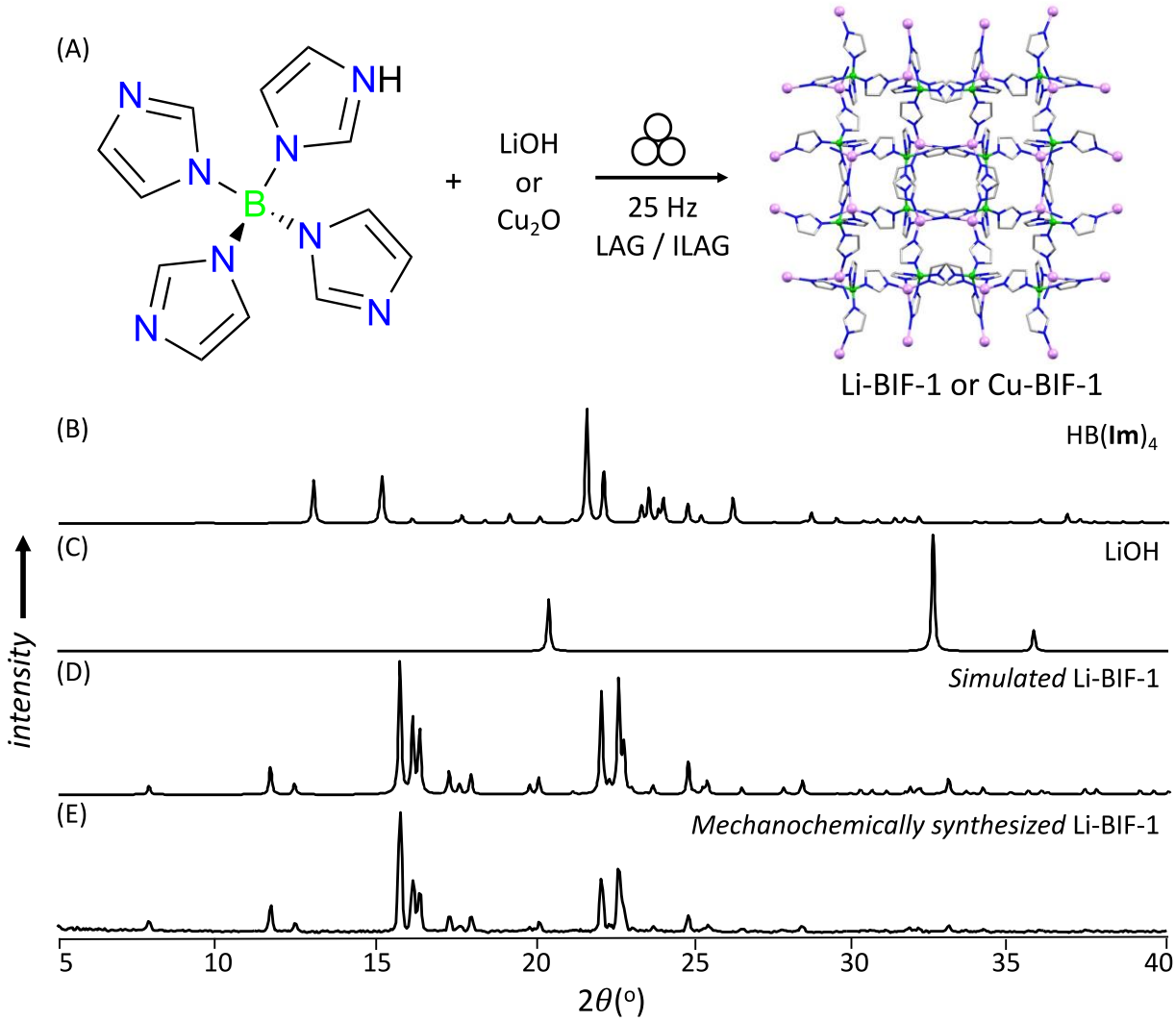

Figure 3. (A) Reaction scheme for the synthesis of Li-BIF-1. Stacked PXRD of (B) H[B(**Im**)$_4$] (C) LiOH, (D) simulated Li-BIF-1 (CSD MOXJPEP) and (E) synthesized BIF-1-Li by LAG for 60 minutes with MeCN (η=0.25 μL mg-1). Corresponding PXRD patterns for the synthesis of Cu-BIF-1 from Cu_2O are given in the ESI.

The acid-base mechanochemical methodology was readily expanded to MOFs based on tetrakis(2-methylimidazole)boric acid H[B(**Meim**)$_4$],[31] previously reported[26] to adopt either a non-porous diamondoid (dia) topology (BIF-2) or a microporous sodalite (SOD) topology (BIF-3) with either Li^+ or Cu^+ as nodes (Figure 4).

Specifically, neat milling of LiOH with a stoichiometric amount of HB(**Meim**)$_4$ led to only a partial and topologically non-selective reaction, with the X-ray powder diffractogram of the milled mixture revealing reflections of residual reactants, along with low-intensity reflections consistent with those calculated for the published[26] structure of the Li-BIF-2 and Li-BIF-3 frameworks (CSD codes MOXKUG and MUCLOM, respectively). Attempts to achieve selective and complete transformation into either BIF-2 or BIF-3 by LAG in the presence of either MeOH or MeCN were not successful, generally resulting in incomplete conversions and/or mixtures of phases (see ESI). Consequently, we explored milling in the presence of 2-aminobutanol (**amb**), which is a ubiquitous component of solvent systems used in the solvothermal syntheses of BIFs.[26,31] Gratifyingly, using a mixture of **amb** and MeCN as the milling liquid led to an effective strategy for the selective synthesis of both the dia-topology Li-

BIF-2, as well as SOD-topology Li-BIF-3. In some cases, the PXRD pattern of the product exhibited Bragg reflections that could not be assigned to neither Li-BIF-2, LiBIF-3, nor any of the reactants (*e.g.*, at $2\theta \approx 6.9^{o}$, see ESI). These were subsequently found to result from the parasitic formation of the hydrated salt [H**amb**$^{+}$][B(**Meim**)$_4^{-}$]·2H_2O, which can be avoided by drying both MeCN and **amb** over molecular sieves before use. In particular, by using a 1:3 by volume mixture of **amb** and MeCN as the grinding liquid and systematically exploring milling times between 15 and 60 minutes, and η values between 0.25 and 1 μL mg^{-1}, revealed that the open framework Li-BIF-3 is readily obtained at η-values of either 0.75 or 1 μL mg^{-1} after grinding for 45 minutes or longer (see ESI). Lower η-values of 0.25 and 0.5 μL mg^{-1} preferred the formation of the dia-topology Li-BIF-2. The phase-pure Li-BIF-2 was obtained upon 60 minutes milling at η=0.5 μL mg^{-1}, following the initial appearance of an as-yet unidentified intermediate phase. The preferred formation of Li-BIF-2 at lower η-values is consistent with our previous observations that lower amounts of liquid promote mechanochemical formation of denser MOF phases.

The formation of phase-pure samples of Li-BIF-2 and Li-BIF-3 was confirmed by PXRD analysis, which revealed an excellent match to diffractograms simulated based on the previously reported structures. (Figure 4B-G) Nitrogen sorption measurement on the mechanochemically obtained Li-BIF-3, after washing with MeCN and evacuation at 85 ^{o}C, revealed a highly microporous material with a Brunauer-Emmet-Teller (BET) surface area of 1010 m^2 g^{-1} (Table 1, Figure 4), which is significantly higher than that previously reported for solvothermally prepared Li-BIF-3 and close to the value expected from the crystal structure of the material.[33] Analysis of the Li-BIF-3 material by scanning electron microscopy (SEM) revealed particles with sizes of hundreds of nanometres, forming larger aggregates several micrometres across (Figure 4).

The analogous copper(I)-based BIF-2 and BIF-3 materials were readily accessible by ILAG, by controlling the volume of the liquid additive and milling time. Similarly to our previous studies of ZIF systems, increased milling times preferred the formation of the close-packed dia-topology Cu-BIF-2. While the PXRD pattern of the reaction mixture after 60 minutes ILAG with MeOH (η=0.5 μL mg-1) and NH_4NO_3 (5 % wt/wt) indicated the presence of the SOD-topology Cu-BIF-3, longer milling led to the appearance of the dia-phase (see ESI). The materials were identified through comparison of experimental PXRD patterns to those simulated for published structures (CSD codes MUCLIG and MOXJOZ for Cu-BIF-2 and Cu-BIF-3, respectively).[26] Quantitative synthesis of Cu-BIF-2 from Cu_2O was readily accomplished by ILAG for 90 minutes (Figure 4H-L). The product after washing and drying was characterized by PXRD, FTIR-ATR, TGA in air and ICP-MS elemental analysis of metal content.

In order to achieve the synthesis of phase-pure microporous Cu-BIF-3, reaction conditions were modified by increasing η to 1 μL mg^{-1}. This modification enabled the reproducible and quantitative synthesis of Cu-BIF-3 (Figure 4H-L), as confirmed by PXRD, FTIR-ATR, TGA and elemental analysis of metal content (see ESI). Nitrogen sorption measurements were performed after washing the mechanochemical product and drying in vacuo at 85 ^{o}C, revealing a high BET surface area of 935 m^2 g^{-1} (Table 1, Figure 4), with individual sub-micron particles, as determined by SEM.

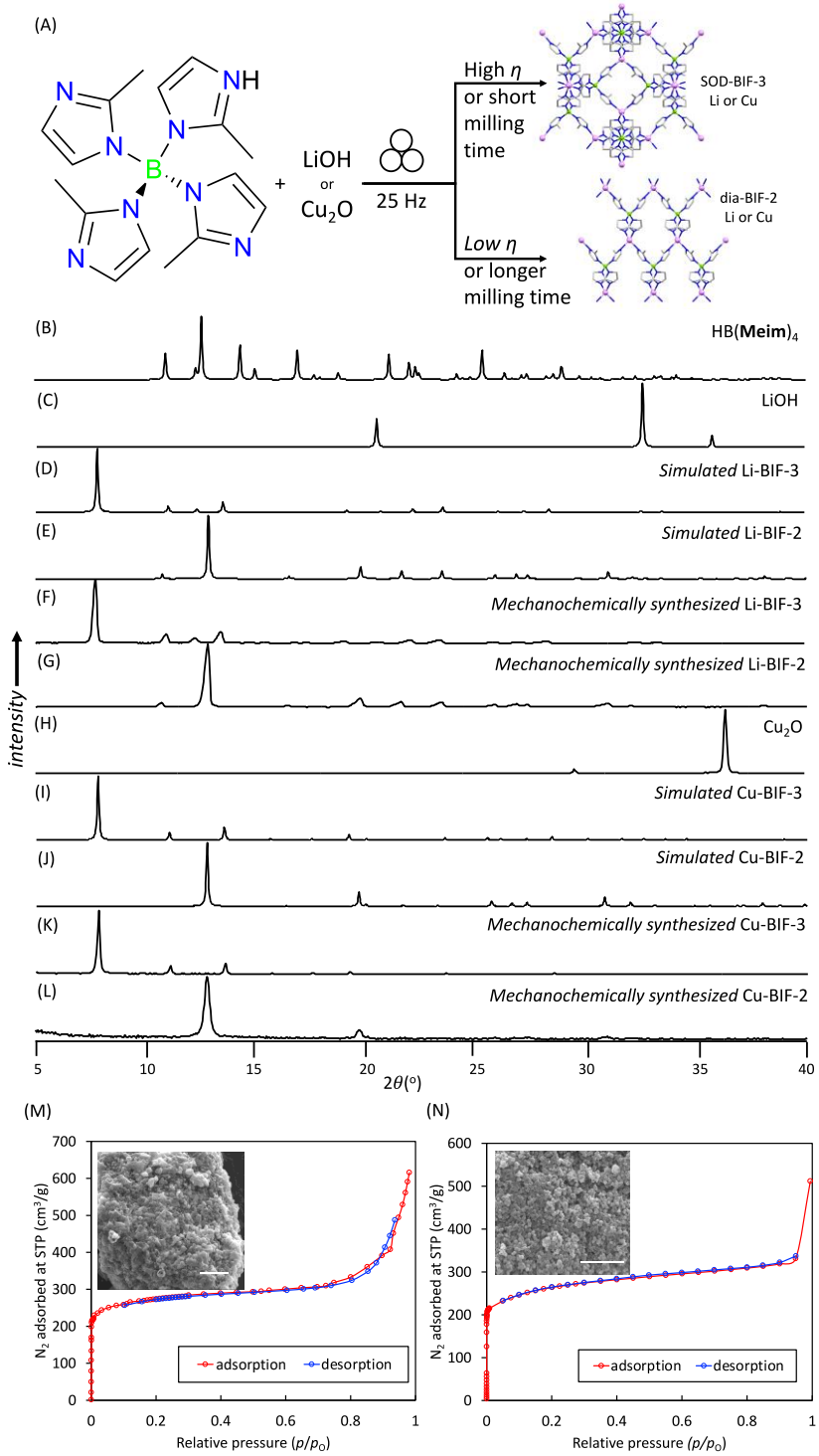

Figure 4. (A) Reaction scheme for the synthesis of Li-BIF-3. Comparison of selected PXRD patterns for: (B) H[B(**Meim**)$_4$ reactant, (C) LiOH reactant, (D) simulated for Li-BIF-3 (CSD MUCLOM), (E) simulated for Li-BIF-2 (CSD MOXKUG), (F) mechanochemically synthesized Li-BIF-3 by LAG for 60 minutes with **amb** and MeCN (η = 1 μL mg^{-1}), and (G) mechanochemically synthesized Li-BIF-2 by LAG for 60 minutes with **amb** and MeCN (η = 0.5 μL mg^{-1}). (H) Cu_2O, (I) Cu-BIF-3 (CSD MOXJOZ) (J) Cu-BIF-2 (CSD MUCLIG), (K) mechanochemically synthesised Cu-BIF-3 by ILAG for 60 minutes with NH_4NO_3 and MeOH (η = 1 μL mg^{-1}), and (L) mechanochemically synthesised Cu-BIF-2 by ILAG for 90 minutes with NH_4NO_3 and MeOH (η = 0.5 μL mg^{-1}). BET adsorption plots for: (M) Li-BIF-3 showing a surface area of 1010 m^2 g^{-1} and (N) Cu-BIF-3 showing a surface area of 935 m^2 g^{-1}. The insets in (M) and (N) are representative SEM images of the samples.

The mechanochemical approaches to Li- and Cu-based BIFs are surprisingly simple compared to previously reported solvothermal methods,[26,31] not only avoiding bulk solvents and high temperatures, but also enabling the use of simple, easily handled solids LiOH and Cu_2O as starting materials compared to, for example, *n*-BuLi. This simplification of the synthetic procedure encouraged us to explore the possibility to extend this family of materials towards previously not reported silver(I) derivatives.

As a starting material for the synthesis of Ag(I)-based BIFs we focused on the inexpensive, readily accessible $AgNO_3$, with K_2CO_3 as a base. One-pot milling reaction of HB(**Meim**)$_4$, $AgNO_3$, and K_2CO_3 in the respective stoichiometric ratios 1:1:½, using MeCN as the milling additive (η=0.25 μL mg^{-1}) readily produced the targeted AgB(**Meim**)$_4$ material along with the side product KNO_3 (Figure 5, also see ESI). Specifically, analysis of the reaction mixtures by PXRD revealed that, similar to the lithium and copper(I) analogues,[26] the silver-based BIF appears in two polymorphs which could be selectively synthesized by varying the milling time. The BIF products were readily separated from the KNO_3 by-product after sequential washing with cold MeOH and acetone, and their respective structures were further validated by structure determination from PXRD data measured on washed and dried materials.

Specifically, milling for 30 minutes led to the formation of a material (Ag-BIF-3) which, based on PXRD analysis, was isostructural to the SOD-topology Li-BIF-3 and Cu-BIF-3. Consequently, the crystal structure of Ag-BIF-3 (Figure 5A) was determined through Rietveld refinement of a structural model based on the Cu-BIF-3 structure, in which the copper(I) sites have been replaced by Ag(I), giving rise to a cubic unit cell (space group *P*-43*n* as in the analogous Cu-BIF-3 and Li-BIF-3 structures) with a = 16.6659(3) Å. Composition of Ag-BIF-3 was verified by TGA/DSC and elemental analysis of metal content (see ESI). The microporous nature of the material was confirmed by N_2 sorption analysis, which revealed a high BET surface area of 1020 m^2 g^{-1}. Sample analysis by SEM revealed dense aggregates of particles, with sizes below 100 nm (Figure 5). The ^{13}C cross-polarisation magic angle spinning (CP-MAS) solid-state nuclear magnetic resonance (ssNMR) spectrum of Ag-BIF-3 was consistent with the crystal structure, revealing three signals in the imidazolate region 100-160 ppm and the -CH_3 group signal at ~16 ppm (Figure 5).

Milling for 60 minutes under otherwise identical conditions led to a material whose PXRD pattern was very similar, but not identical, to that of dia-topology Li-BIF-2 and Cu-BIF-2 materials, with additional Bragg reflections indicating possible lower symmetry. The structure of this material (Figure 5B) was determined by simulated annealing structure solution from PXRD data, revealing a monoclinic (space group $P2_1$) unit cell with a = 7.5198(4) Å, b = 16.3763(9) Å, c = 7.5876(4) Å and β = 90.136(6)°. In contrast to structures of Li-BIF-2 and Cu-BIF-2, which all exhibited one symmetrically independent **Meim**$^-$ ligand in a tetragonal *I*-4 space group, the structure of Ag-BIF-3 displays each tetrahedral node surrounded by four symmetrically non-equivalent imidazolate ligands. This much higher multiplicity is clearly reflected by the ssNMR spectrum of the material, validating the structure (Figure 5). The composition of the material was similarly confirmed by TGA and by elemental analysis of the metal content (see ESI). For both Ag-BIF-2 and Ag-BIF-3 the measured ^{13}C ssNMR chemical shifts were consistent with those calculated from the herein determined crystal structures (Figure 5D-G).

Notably, while materials based on silver(I) ions are often expected to be light sensitive, the herein reported Ag-BIF-2 and Ag-BIF-3 both appeared unchanged following six months exposure storage in a transparent vial on the bench.

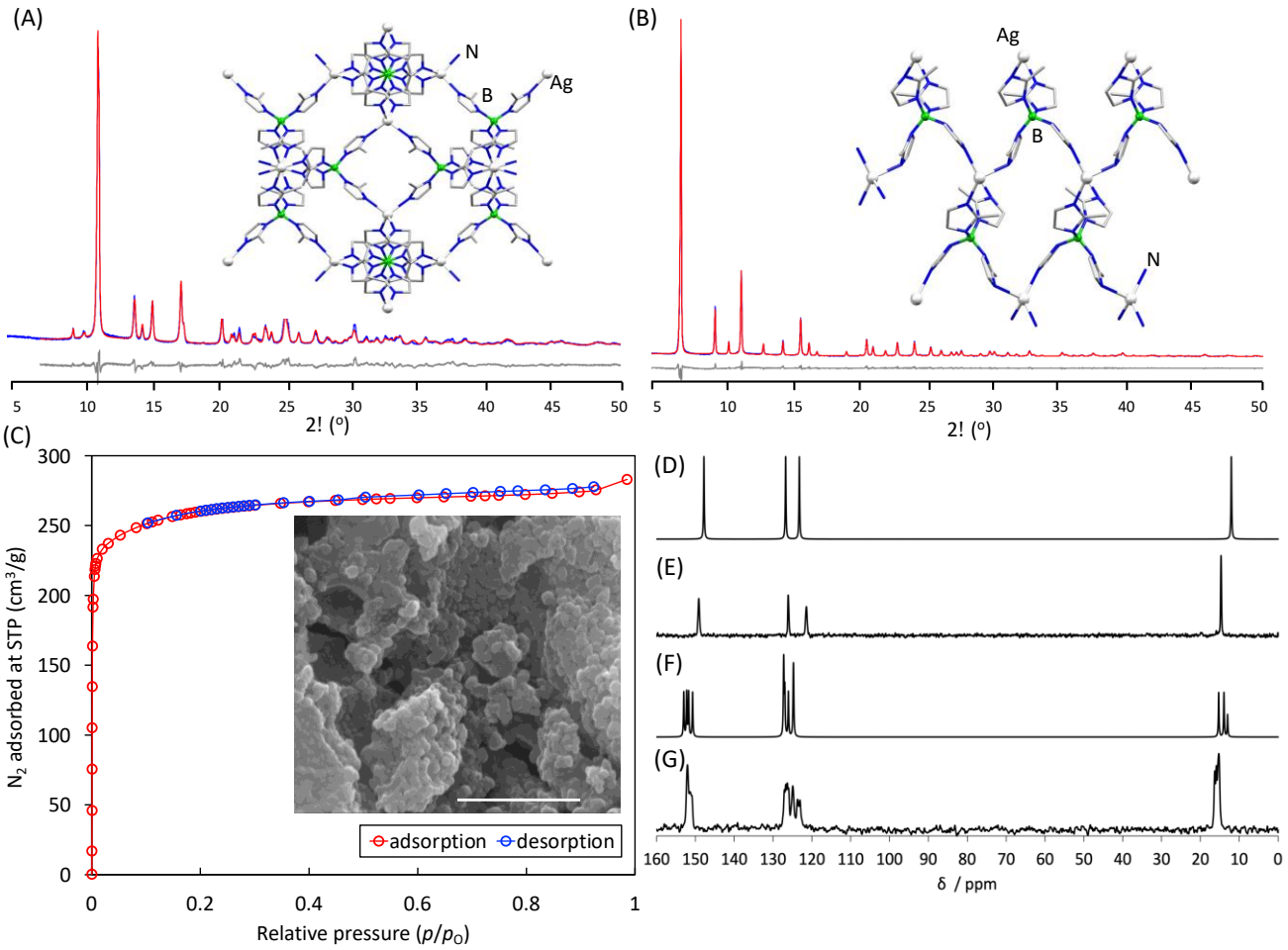

Figure 5. (A) Rietveld refinement of Ag-BIF-3 with difference plot shown in grey. (B) Rietveld refinement of Ag-BIF-2 with difference plot shown in grey. (C) BET adsorption plot Ag-BIF-3 showing a surface area of 1020 m^2 g^{-1} and a SEM image of a representative sample (scale-bar 1 μm). Comparison of measured and simulated ^{13}C CP-MA ssNMR spectra for silver-based BIFs: (D) calculated for Ag-BIF-3, (E) measured for Ag-BIF-3, (F) calculated for Ag-BIF-2 and (G) measured for Ag-BIF-2.

The crystal structures of Li-, Cu- and Ag-based BIFs provide a unique opportunity to evaluate the effect of changes in the metal node on the relative stability of BIF polymorphs with SOD- and dia-topology across three metals.[35–37] The calculations were done using CASTEP plane-wave density-functional theory (DFT)[38] code. The previously published crystal structures of Li- and Cu-BIFs with Meim- linkers, as well as the structures of Ag-BIFs herein determined, were geometry-optimized using the PBE[39] functional combined with many-body dispersion (MBD*)[40–42] correction scheme. The PBE+MBD* approach has previously shown excellent agreement with experimental calorimetric measurements of ZIF polymorphs,[24] therefore we expected the same approach to perform reliably for the structures of BIFs. In addition to calculating the relative energies of SOD- and dia-polymorphs, we have performed Gauge Including Projector Augmented Waves (GIPAW)[43] simulation of the solid-state NMR spectra of Ag-BIFs to compare the simulated spectra with their experimental counterparts, confirming the low symmetry Ag-BIF-2 structure derived from PXRD data (Figure 5D-E).

Table 1. Experimental Brunauer-Emmet-Tellet (BET) and Langmuir surface areas of mechanochemically synthesized SOD-topology BIFs, compared to previously measured and theoretically calculated surface area (SA) values, along with average particle sizes established by SEM and calculated energies (in eV) for Li-, Cu-, and Ag-BIF polymorphs. The difference between calculated energies for SOD- and dia-polymorphs is given as ΔE, in kJ mol^{-1}.

Material	Mechanochemical, BET ($m^2\ g^{-1}$)	Mechanochemical, Langmuir ($m^2\ g^{-1}$)	Previously reported SA, Langmuir ($m^2\ g^{-1}$)[26]	Calculated SA ($m^2\ g^{-1}$)[a]	Electronic energy per formula unit (eV)	ΔE (kJ mol^{-1})	Particle size (nm)[b]
dia-$Li_{0.5}B_{0.5}$(**Meim**)$_2$	-	-	-	-	-2679.174		
SOD-$Li_{0.5}B_{0.5}$(**Meim**)$_2$	1010	1060	762.5	1200	-2679.026	14.25	217 (*n*=24)
dia-$Cu_{0.5}B_{0.5}$(**Meim**)$_2$	-	-	-	-	-3417.091		
SOD- $Cu_{0.5}B_{0.5}$(**Meim**)$_2$	935	1196	182.3	1100	-3416.991	9.67	611 (*n*=500)
dia-$Ag_{0.5}B_{0.5}$(**Meim**)$_2$	-	-	-	-	-4738.959	8.66	500 (*n*=25)
SOD-$Ag_{0.5}B_{0.5}$(**Meim**)$_2$	1020	1205	-	1170	-4738.869		

[a]Calculated using MOF Explorer (see ESI); [b]Determined from SEM measurements, where *n* corresponds to number of particles observed.

Comparison of calculated energies reveals that increasing the atomic number of the metal node results in increased stabilization of the SOD-topology open framework with respect to the close-packed dia-polymorph. The energy differences are shown as ΔE in Table 1. Specifically, whereas Li-BIF-3 structure is calculated to be ca. 14 kJ mol^{-1} less stable compared to its dia-counterpart, the corresponding differences for Cu-BIF-3 and Ag-BIF-3 are calculated to be considerably smaller, at 9.7 kJ mol^{-1} and 8.7 kJ mol^{-1}, respectively. The calculated energies are in a similar range to the calculated (15.2 kJ mol^{-1}) and measured (10.6 kJ mol^{-1}) ones for the analogous zinc-based ZIFs, indicating that switching between transition metal and main group-based nodes, or switching between using only a divalent node and a combination of monovalent and trivalent nodes, does not significantly influence the difference in stability of SOD- and dia-topology frameworks. The improvement in the relative stability of open BIF structure upon switching from Li^+ to Cu^+ and Ag^+ nodes is notable, considering the recent interest in the development of MOFs based on heavy-atom nodes.[44-46]

The simulated ssNMR spectra of Ag-BIF-2 and Ag-BIF-3 showed excellent agreement with the experiment (Figure 5) in terms of overall chemical shift and the number of distinct NMR peaks arising from the crystallographic symmetry. The spectrum of the SOD polymorph is consistent with a single symmetrically unique **Meim**$^-$ linker, while the peak splitting found in the spectrum of the dia-polymorph corresponds to four distinct 2-methylimidazolate units. The NMR simulation fully supports the structural models derived from PXRD data, with calculated chemical shifts underlining the accuracy of the herein used theoretical approach.

In summary, we have shown that the application of mechanochemical methodologies can greatly simplify the synthesis of zeolitic boron imidazolate frameworks, providing a rapid, room-temperature approach to this class of materials, using simple metal oxide or hydroxide reactants. Contrary to previously reported materials obtained by solvothermal synthesis, the open framework SOD topology BIFs made mechanochemically show higher surface areas, that are very close to the theoretically calculated ones. The use of mechanochemistry also expanded the scope of the zeolitic BIF class of materials, by enabling the synthesis of previously not reported silver-based systems. Theoretical investigation of isostructural BIFs based on Li^+, Cu^+ and Ag^+ reveals that the use of increasingly heavier tetrahedral metal nodes leads to the stabilization of open-framework SOD-topology structure with respect to the corresponding close-packed dia polymorph. Overall, the presented results and synthetic methodologies should provide simpler, faster access to an intriguing, but so far poorly developed, class of ultralight zeolitic MOFs.

Acknowledgments
We acknowledge support of NSERC Discovery Grant (RGPIN-2017-06467), Discovery Accelerator Award (RGPAS 507837-17), Strategic Grant (STPGP 521582-18), and PGS-D Scholarship (to C.B.L.). MA thanks the National Science Center of Poland (NCN) for the support via SONATA grant (2018/31/D/ST5/03619). We also thank PL-Grid for access to the Prometheus supercomputer. Dr Robin S. Stein is acknowledged for help in acquiring NMR data.

References
1 S. L. James, C. J. Adams, C. Bolm, D. Braga, P. Collier, T. Friščić, F. Grepioni, K. D. M. Harris, G. Hyett, W. Jones, A. Krebs, J. Mack, L. Maini, A. G. Orpen, I. P. Parkin, W. C. Shearouse, J. W. Steed and D. C. Waddell, *Chem. Soc. Rev.*, **2012**, *41*, 413-447.
2 T. Friščić, C. Mottillo and H. M. Titi, *Angew. Chem. Int. Ed.*, **2020**, *13*, 1018–1029.
3 N. R. Rightmire and T. P. Hanusa, *Dalton Trans.*, **2016**, *45*, 2352-2362.
4 E. Boldyreva, *Chem. Soc. Rev.*, **2013**, *42*, 7719–7738.
5 A. Porcheddu, E. Colacino, L. De Luca and F. Delogu, *ACS Catal.*, **2020**, *10*, 8344-8394.
6 J. M. Andersen and J. Mack, *Chem. Sci.*, **2017**, *8*, 5447-5453.
7 C. Bolm and J. G. Hernández, *Angew. Chem. Int. Ed.*, **2019**, *58*, 3285-3299.
8 P. Baláž, M. Achimovičová, M. Baláž, P. Billik, Z. Cherkezova-Zheleva, J. M. Criado, F. Delogu, E. Dutková, E. Gaffet, F. J. Gotor, R. Kumar, I. Mitov, T. Rojac, M. Senna, A. Streletskii and K. Wieczorek-Ciurowa, *Chem. Soc. Rev.*, **2013**, *42*, 7571-7637.
9 B. G. Fiss, N.-N. Vu, G. Douglas, T.-O. Do, T. Friščić and A. Moores, *ACS Sustain. Chem. Eng.*, **2020**, *8*, 12014-12024.
10 D. Prochowicz, M. Saski, P. Yadav, M. Grätzel and J. Lewiński, *Acc. Chem. Res.*, **2019**, *52*, 3233-3243.
11 D. DeSantis, J. A. Mason, B. D. James, C. Houchins, J. R. Long and M. Veenstra, *Energy & Fuels*, **2017**, *31*, 2024-2032.
12 T. Stolar and K. Užarević, *CrystEngComm*, **2020**, *22*, 4511-4525.
13 R. Riccò, O. Linder-Patton, K. Sumida, M. J. Styles, K. Liang, H. Amenitsch, C. J. Doonan and P. Falcaro, *Chem. Mater.*, **2018**, *30*, 5630–5638.
14 D. Crawford, J. Casaban, R. Haydon, N. Giri, T. McNally and L. S. James, *Chem. Sci.*, **2015**, *6*, 1645-1649.
15 K. Užarević, T. C. Wang, S. Y. Moon, A. M. Fidelli, J. T. Hupp, O. K. Farha and T. Friščić, *Chem. Commun.*, **2016**, *52*, 2133–2136.
16 A. D. Katsenis, A. Puškarić, V. Štrukil, C. Mottillo, P. A. Julien, K. Užarević, M. H. Pham, T. O. Do, S. A. J. Kimber, P. Lazić, O. Magdysyuk, R. E. Dinnebier, I. Halasz and T. Friščić, *Nat. Commun.*, **2015**, *6*, 6662.
17 M. Arhangelskis, A. D. Katsenis, N. Novendra, Z. Akimbekov, D. Gandrath, J. M. Marrett, G. Ayoub, A. J. Morris, O. K. Farha, T. Friščić and A. Navrotsky, *Chem. Mater.*, **2019**, *31*, 3777-3783.
18 W. Xu, H. Chen, K. Jie, Z. Yang, T. Li and S. Dai, *Angew. Chem. Int. Ed.*, **2019**, *58*, 5018-5022.
19 D. E. Crawford and J. Casaban, *Adv. Mater.*, **2016**, *28*, 5747-5754.
20 A. A. L. Michalchuk, K. S. Hope, S. R. Kennedy, M. V. Blanco, E. V. Boldyreva and C. R. Pulham, *Chem. Commun.*, **2018**, *54*, 4033–4036.
21 H. M. Titi, J.-L. Do, A. J. Howarth, K. Nagapudi and T. Friščić, *Chem. Sci.*, **2020**, *11*, 7578-7584.
22 P. A. Julien, C. Mottillo and T. Friščić, *Green Chem.*, **2017**, *19*, 2729-2747.
23 T. Friščić and L. Fábián, *CrystEngComm*, **2009**, *11*, 743-745.

24 Z. Akimbekov, A. D. Katsenis, G. P. Nagabhushana, G. Ayoub, M. Arhangelskis, A. J. Morris, T. Friščić and A. Navrotsky, *J. Am. Chem. Soc.*, **2017**, *139*, 7952–7957.
25 N. Novendra, J. M. Marrett, A. D. Katsenis, H. M. Titi, M. Arhangelskis, T. Friščić and A. Navrotsky, *J. Am. Chem. Soc.*, **2020**, *142*, 21720-21729.
26 J. Zhang, T. Wu, C. Zhou, S. Chen, P. Feng and X. Bu, *Angew. Chem. Int. Ed.*, **2009**, *48*, 2542-2545.
27 M. Klimakow, P. Klobes, A. F. Thünemann, K. Rademann and F. Emmerling, *Chem. Mater.*, **2010**, *22*, 5216-5221.
28 T. Wu, J. Zhang, C. Zhou, L. Wang, X. Bu and P. Feng, *J. Am. Chem. Soc.*, **2009**, *131*, 6111-6113.
29 V. I. Isaeva, K. E. Papathanasiou and L. M. Kustov, *Crystals*, **2020**, *10*, 617.
30 T. Friščić, S. L. Childs, S. A. A. Rizvi and W. Jones, *CrystEngComm*, **2009**, *11*, 418–426.
31 P. J. Bailey, D. Lorono-Gonzales, C. McCormack, F. Millican, S. Parsons, R. Pfeifer, P. P. Pinho, F. Rudolphi and A. Sanchez Perucha, *Chem. Eur. J.*, **2006**, *12*, 5293–5300.
32 T. Friščić, I. Halasz, P. J. Beldon, A. M. Belenguer, F. Adams, S. A. J. Kimber, V. Honkimäki and R. E. Dinnebier, *Nat. Chem.*, **2013**, *5*, 66–73.
33 T. Friščić, D. G. Reid, I. Halasz, R.S. Stein, R. E. Dinnebier and M. J. Duer, *Angew. Chem. Int. Ed.*, **2010**, *49*, 712-715.
34 P. J. Beldon, L. F. Fabain, R. S. Stein, A. Thirumurugan, A. K. Cheetham, T. Friščić, *Angew. Chem. Int. Ed.*, **2010**, *49*, 9640-9643.
35 R. Galvelis, B. Slater, A. K. Cheetham and C. Mellot-Draznieks, *CrystEngComm*, **2012**, *14*, 374–378.
36 C. Mellot-Draznieks and B. Kerkeni, *Mol. Simul.*, **2014**, *40*, 25–32.
37 I. A. Baburin and S. Leoni, *J. Mater. Chem.*, **2012**, *22*, 10152–10154.
38 S. J. Clark, M. D. Segall, C. J. Pickard, P. J. Hasnip, M. I. J. Probert, K. Refson and M. C. Payne, *Z. Krist.*, **2009**, *220*, 567-570.
39 A. Vela, J. C. Pacheco-Kato, J. L. Gázquez, J. M. del Campo and S. B. Trickey, *J. Chem. Phys.*, **2012**, *136*, 144115.
40 A. Tkatchenko, R. A. DiStasio, R. Car and M. Scheffler, *Phys. Rev. Lett.*, **2012**, *108*, 236402.
41 A. Ambrosetti, A. M. Reilly, R. A. DiStasio and A. Tkatchenko, *J. Chem. Phys.*, **2014**, *140*, 18A508.
42 A. M. Reilly and A. Tkatchenko, *Chem. Sci.*, **2015**, *6*, 3289–3301.
43 J. R. Yates, C. J. Pickard and F. Mauri, *Phys. Rev. B*, **2007**, *76*, 024401.
44 K. P. Carter, J. A. Ridenour, M. Kalaj, C. L. Cahill, *Chem. Eur. J.* **2019**, *25*, 7114-7118.
45 S. E. Gilson, P. Li, J. E. S. Szymanowski, J. White, D. Ray, L. Gagliardi, O. K. Farha, P. C. Burns, *J. Am. Chem. Soc.* **2019**, *141*, 11842-11846.
46 I. R. Speight, I. Huskic, M. Arhangelskis, H. M. Titi, R. S. Stein, T. P. Hanusa, T. Friščić, *Chem. Eur. J.* **2020**, *26*, 1811-1818.